Solvent-induced high-spin transition in double-decker 3*d*-4*f* metallacrowns

A. Alhassanat,[1] L. Völker,[2] C. Gamer,[2] A. Rauguth,[2] A. Kredel,[2] C. Luo,[3,4] F. Radu,[3] A. A. Sapozhnik,[1] T. Mashoff,[1] E. Rentschler,[2] and H. J. Elmers[1,*]

[1]*Institut für Physik, Johannes Gutenberg-Universität, Staudingerweg 7, D-55099 Mainz, Germany*

[2]*Institut für Anorganische und Analytische Chemie, Universität Mainz, D-55128 Mainz, Germany*

[3]*Helmholtz-Zentrum Berlin für Materialien und Energie, Albert-Einstein Str. 15, D-12489, Berlin, Germany*

[4]*Institut für Experimentelle und Angewandte Physik, Universität Regensburg, Universitätsstrasse 31, D-93053 Regensburg, Germany*

(Received 8 August 2018; revised manuscript received 20 February 2019; published 4 March 2019)

Element-specific magnetic spin and orbital magnetic moments of 3*d*-4*f* double-decker metallacrown molecules have been investigated using x-ray magnetic circular dichroism. The double-decker metallacrowns comprise one rare-earth Gd(III) or Tb(III) ion embedded between two squared scaffolds of four Ni(II) ions. We observe a strong increase of the Ni(II) moments if the molecules are dissolved in methanol, indicating a spin crossover from a low-spin to a high-spin state. In contrast, dichloromethane does not change the spin state. This result is explained by a change of the coordination environment of nickel. The comparison of charge-transfer multiplet calculations with the experimental absorption spectra confirm the different ligand fields.

DOI: 10.1103/PhysRevB.99.104404

I. INTRODUCTION

Molecular spintronics has become an interesting research topic because of its high potential in processing and transport of information, aiming at replacing conventional electronics by bottom-up technologies [1]. In this field, bistable spin states occurring in the 3*d* transition metal ions with d^4 to d^7 orbital occupancy play an important role. Switching these spin states by external parameters [2–12] provides control over the interaction of electron spins within a single molecule.

The 3*d* metal ion's spin state may assume different spin configurations resulting in different numbers of unpaired *d* electrons. Within the simplest approach, the spin state depends on the ligand field strength. For intermediate field strength, where both configurations are of similar energy, the spin multiplicity changes with temperature or pressure due to entropic effects. This is the case of the spin crossover transition according to the definition given in Ref. [13].

Classical spin-crossover complexes involve Fe(II) ions [3], where an entropy-driven transition from a paramagnetic high-spin state to a diamagnetic low-spin state occurs. Boundary restrictions such as metallic surfaces may significantly change the spin-crossover behavior as has been shown for $[Fe(phen)_2(NCS)_2]$ [14]. Ni(II) systems may also show a thermally induced transition between bistable diamagnetic and paramagnetic spin states [15], where the transition is caused by a change of coordination from the square-planar (diamagnetic) ligand field to an octahedral (paramagnetic) ligand field.

Besides spin crossover, transitions between bistable states of different multiplicities may also be induced by external variation of ligand fields. Reference [16] reports a bistable molecular Ni(II) spin switch induced by a light-induced coordination change. Recently, the role of ligand fields in influencing the spin crossover [17,18], phase transition and photoswitching [19–21], charge transport and electrical properties [22], and guest effects on spin crossover in Hoffmann-type metal-organic frameworks [23] has been reviewed.

Using x-ray absorption spectroscopy ligand-field-induced changes of magnetic moments have been investigated for several systems [24,25]. By time-resolved x-ray absorption spectroscopy Chen *et al.* [26] measured photoexcited changes of spin states with high temporal resolution. Duval *et al.* [27] observed spin-state changes in the β-pyrrole-substituted Ni(II)-porphyrins induced by coordination variation. Wäckerlin *et al.* [28] applied x-ray absorption spectroscopy to investigate the occurrence of magnetic moments in Ni(II)-porphyrine caused by ammonia coordination.

Heteronuclear 3*d*-4*f* molecular complexes comprising bistable spin states provide interesting magnetic properties. In particular, combinations with the rare-earth ions Tb(III) and Dy(III) are promising components for molecular magnets. The 4*f* ions potentially enhance the molecular magnetic anisotropy leading to slow relaxation rates and single-molecule magnet (SMM) behavior [29–39]. Heteronuclear 3*d*-4*f* single-molecule magnets [40–44] have been synthesized with anisotropy barriers even higher than those for 3*d*-only complexes.

Metallacrowns represent multinuclear cyclic metal clusters, with a structure comparable to the organic crown ethers consisting of [M–N–O] repeating units. Some molecules of this group show SMM behavior. [45–47] The interaction between the single-ion electron density and the crystal field leads to an enhancement of the energy barrier for the magnetization reversal [48]. Understanding the particular crystal field environment is important for the optimization of the slow-relaxation properties in metallacrowns. In this article we exploit the high integrity and thermodynamic stability in solution of hetero-nuclear metallacrowns forming a double-decker

*elmers@uni-mainz.de

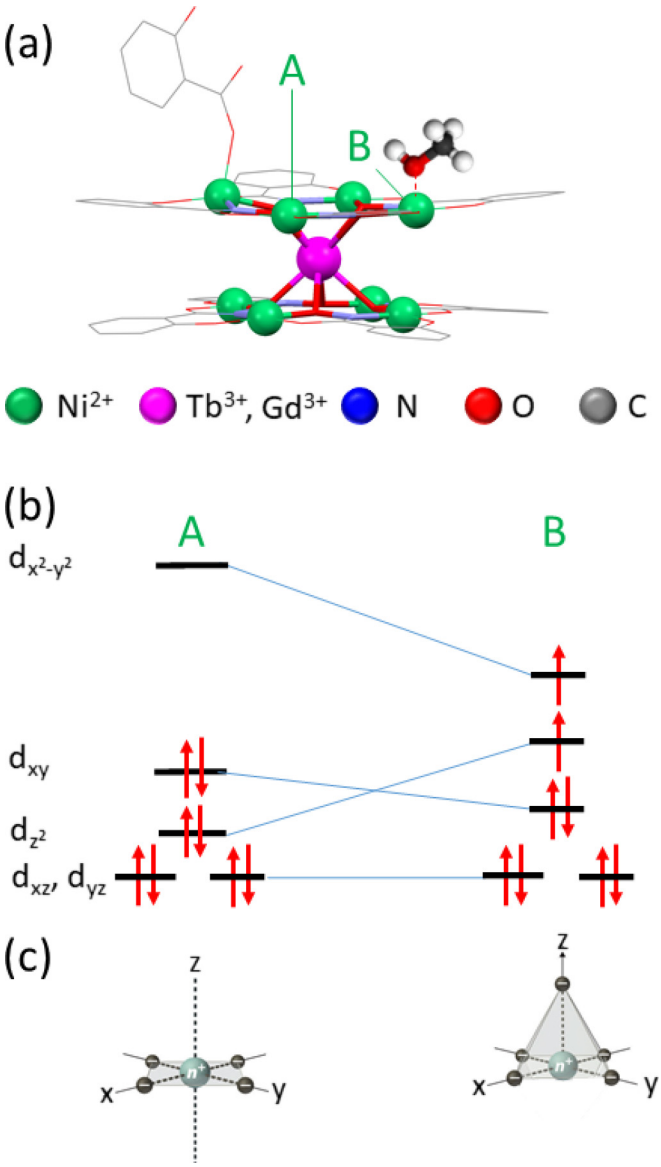

FIG. 1. (a) Molecular structure of the $\{TbNi_8\}$ molecule. Site A indicates a Ni(II) ion within a square-planar ligand field as determined by x-ray diffraction from a single crystal. Site B sketches the assumed structure with methanol molecules attached along the z axis after solving in methanol and subsequent drying in vacuum. (b) Scheme of the splitting of the Ni(II) d orbitals in the square-planar field (site A), resulting in the low-spin state $S = 0$. In an octahedral or tetragonal extended ligand field (site B) the intra-atomic exchange interaction (Hund's rule) favors the high-spin state $S = 1$. (c) Sketch of the square-planar ligand field and the tetragonal extended ligand field.

structure comprising one rare-earth Gd(III) or Tb(III) ion embedded between two squared scaffolds of four Ni(II) ions.

The analysis of magnetic properties of heterometallic $3d$-$4f$ molecules is challenging [44] because intramolecular coupling and the ground-state total angular momentum are masked by the dominant effect of the ligand field splitting [49–51]. X-ray magnetic circular dichroism (XMCD) provides element-specific information and thus helps to understand the complex magnetic behavior of $3d$-$4f$ magnetic molecules [25,52–59,59–65].

While previous studies of $3d$-$4f$ metallacrown complexes have focused on the properties of the rare-earth ions [66], we mainly explore here the properties of the $3d$ Ni(II) ions. The structure of the molecule implies a square-planar ligand field that is expected to lead to a $S = 0$ ground state, i.e., a vanishing Ni moment. Deviations from the square-planar ligand field as, for example, caused by additional coordinating molecules may switch the Ni(II) ion to a high-spin $S = 1$ state for the d^8-electron configuration. We investigate by XMCD the effect of this chemically induced spin crossover on the magnetic properties of double-decker metallacrowns [see Fig. 1(a)] comprising a central rare-earth ion either with or without an orbital moment.

II. EXPERIMENT

$(Hpip)_6\{RE\{(III)[12\text{-}MC_{Ni(II)N(shi)}\text{-}4]_2(Hsal)\}$, shi = salicylhydroxamic acid (in short $\{RENi_8\}$), molecules with RE = Gd and Tb have been synthesized as described in Ref. [67]. The structures of the molecules have been determined by x-ray diffraction of single crystals. XMCD measurements were carried out at the VEKMAG endstation of the PM2 beamline at BESSY II [68]. The degree of circular polarization is $P = 0.77$. X-ray absorption spectra (XAS) at the Ni $L_{3,2}$ and RE $M_{5,4}$ edges result from the total electron yield as measured by the sample current at 7 K. A magnetic field of 7 T was applied parallel and antiparallel to the incident photon beam with the sample oriented perpendicular to the magnetic field. The difference of the two XAS spectra results in the XMCD. Even after several hours of absorption measurements we did not detect any changes of the spectra, indicating that no radiation damage of the molecules occurred. For the XMCD measurements the $\{RENi_8\}$ molecules were deposited on a silicon wafer surface prior to the transfer into ultrahigh vacuum. We applied three different methods for the deposition. Ultrasmall crystals (powder) were glued to the Si wafer surface by a mixture of graphite powder and xylol (conductive carbon cement). Because the insulating crystals partially charge up during the measurement, the total electron yield current is in the range of only 0.1 pA and long-acquisition times are needed to reduce the signal noise. Therefore, in a second approach we deposited the molecules by drop-casting from a dichloromethane solution, resulting in sample currents in the range of several picoamperes. Both methods lead to similar spectral features. In a third approach the molecules were drop-cast from a methanol solution. This deposition method leads to a considerable change of the Ni spectra, as is discussed below.

Element-specific magnetic moments were determined by the sum-rule analysis [69,70]. The applicability of such rules requires some arbitrary assumptions concerning the number of $3d$ and $4f$ holes, the jj mixing effect, and the dipolar term $\langle \mathbf{T}_z \rangle$ [71]. We have set the number of d holes to the values as determined by charge-transfer multiplet calculations [72] and the number of f holes to the ionic values. The jj-mixing effect is considered as a correction factor for the magnetic spin moment. The correction factor is 1 in the case of the Ni(II) and RE(III) ions because of the comparatively large spin-orbit splitting of the initial states. The expectation value of the dipole operator $T_z = \langle \mathbf{T}_z \rangle$ contributes to the

effective spin moment for transition-metal and rare-earth ions. T_z only vanishes in the case of Gd(III) and Eu(II) and it is large in the case of Tb(III) (see Refs. [69,70]). In the case of rare-earth ions it can be calculated exactly according to Ref. [69]. The angular dependence of T_z can be described by the Legendre polynomial $(1 - 3\cos^2\theta)$ [73,74]. An important precondition for the occurrence of this angular dependence is that the quadrupolar charge distribution remains largely unaffected by the magnetic spin orientation. We assume that this precondition is fulfilled in our case because the spin-orbit coupling is smaller than the bandwidth for the valence states of $3d$ and $4f$ metal ions. The quadrupolar charge distribution results in $\langle T_x\rangle + \langle T_y\rangle + \langle T_z\rangle = 0$: Consequently, T_z vanishes for powder samples in the case of a saturated magnetic state, i.e., for the external fields being much larger than the magnetic anisotropy fields (see Refs. [74,75]). In contrast, for an external field much smaller than the magnetic anisotropy field, the exact result of T_z for RE(III) ions can be used to determine the spin moment [44]. The intermediate case of anisotropy and external fields being of equal size is discussed in Ref. [66].

III. RESULTS

Figure 2 shows the XAS and XMCD spectra of the {$GdNi_8$} samples. The XAS Ni L_3 edge at a photon energy

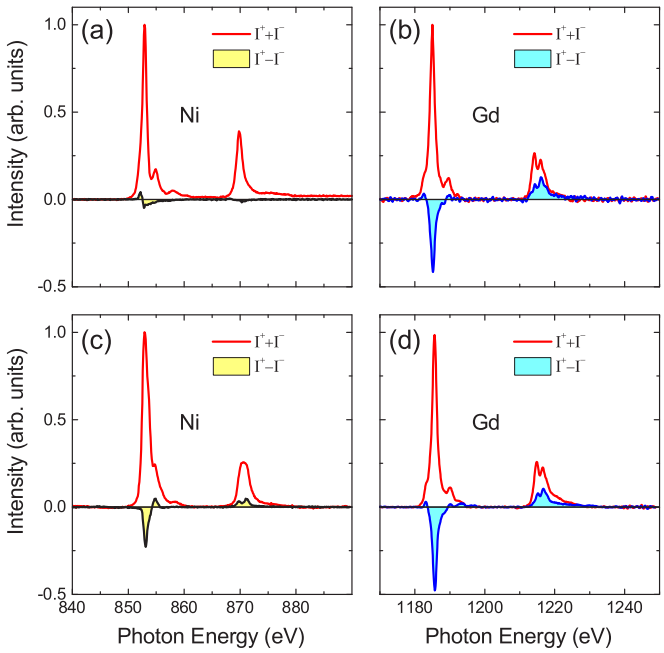

FIG. 2. The x-ray absorption $I^+ + I^-$ and XMCD $I^+ - I^-$ spectra measured at the Ni $L_{3,2}$ and Gd $M_{5,4}$ edges for the {$GdNi_8$} metallacrowns. Panels (a) and (b) respectively show XAS and XMCD spectra for {$GdNi_8$} deposited by drop-casting from a solution in dichloromethane. Panels (c) and (d) respectively show XAS and XMCD spectra for {$GdNi_8$} deposited by drop-casting from a solution in methanol. I^+ and I^- denote the total photoemission yield measured for the external fields parallel and antiparallel to the circular polarization vector of the synchrotron light. The XAS spectra for Ni(II) [panels (a) and (c)] and Gd(III) [panels (b) and (d)] are normalized to the maximum value. The corresponding XMCD spectra are scaled by the same normalization factor.

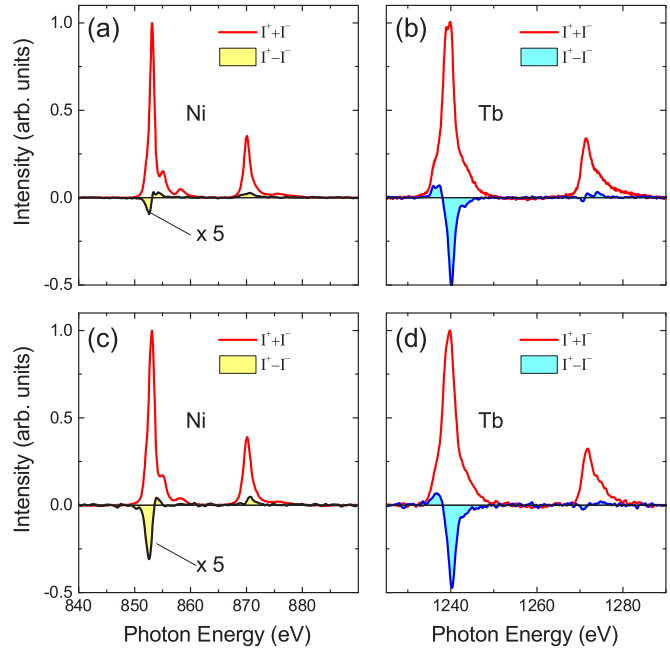

FIG. 3. The x-ray absorption $I^+ + I^-$ and XMCD $I^+ - I^-$ spectra measured at the Ni $L_{3,2}$ and RE $M_{5,4}$ edges for the {$TbNi_8$} metallacrowns. Panels (a) and (b) respectively show the XAS and XMCD spectra for {$TbNi_8$} deposited by drop-casting from a solution in dichloromethane. Panels (c) and (d) respectively show XAS and XMCD spectra for {$TbNi_8$} deposited by drop-casting from a solution in methanol. I^+ and I^- denote the total photoemission yield measured for the external fields parallel and antiparallel to the circular polarization vector of the synchrotron light. The XAS spectra for Ni(II) [panels (a) and (c)] and Tb(III) [panels (b) and (d)] are normalized to the maximum value. The corresponding XMCD spectra are scaled by the same normalization factor. The Ni(II) XMCD spectra [panels (a) and (c)] are magnified by a factor of 5.

of 853 eV reveals two additional satellite peaks at 2 and 5 eV higher than the energy of the absorption maximum. The XAS spectra measured for the sample drop-cast from the dichloromethane solution [Fig. 2(a), case A] deviates from the spectra measured for the same molecules drop-cast from a methanol solution [Fig. 2(c), case B]. For case A the satellite peak at 855 eV is smaller and the shift from the main peak is larger (2.0 eV) compared to case B (1.8 eV). The larger separation from the main peak in case A leads to a clear satellite peak, while in case B the additional peak rather forms a shoulder on the high-energy side of the main peak. A second prominent difference occurs at the L_2 edge at a photon energy of 870 eV. For case A we observe a narrow peak almost half the size of the L_3 peak. In contrast, case B reveals a smaller maximum peak value and the width of the peak is enhanced.

The most obvious difference occurs for the Ni XMCD signal. In case A the XMCD signal is very small and it reveals a plus/minus feature at the L_3 edge (853 eV). Drop-casting from methanol, instead, results in a much larger XMCD signal, showing a prominent negative peak at the L_3 edge and a positive peak at the L_2 edge. Thus, the XMCD signal indicates a prevailing spin moment parallel to the applied external field.

The XAS and XMCD signals measured at the Gd(III) $M_{5,4}$ edge are similar for both cases A and B [Figs. 2(b)

TABLE I. Effective spin moment $\mu_{\text{spin}}^{\text{eff}}$ and orbital moment μ_{orb} in units of Bohr magnetons (μ_{B}) as determined by the sum rules for $\{GdNi_8\}$ and $\{TbNi_8\}$ at 7 K for a field of 7 T. $\{RENi_8\}$ denotes case A of the samples drop-cast from a dichloromethane solution, and $\{RENi_8\} \cdot CH_3OH$ indicates case B of the samples drop-cast from a methanol solution. The total Ni(II) magnetic moment results from $\mu_{\text{tot}} = \mu_{\text{spin}}^{\text{eff}} + \mu_{\text{orb}}$. In the case of Tb(III) the actual spin moment μ_{spin} is larger than $\mu_{\text{spin}}^{\text{eff}}$ because of the T_z contribution as discussed in the text. The molecular moment μ_{mol} calculated from the XMCD sum rule results from the composition of the molecule $\mu_{\text{mol}} = 8\mu_{\text{tot}}(\text{Ni}) + \mu_{\text{tot}}(RE)$. The error of the XMCD-derived moments is dominated by systematic errors of the common factors' polarization, n_h, and the error due to subtraction of transitions into continuous states. We estimate the total error to be on the order of 20%.

	Ni(II)			*RE*(III)		Mol. moments
	$\mu_{\text{spin}}^{\text{eff}}$	μ_{orb}	μ_{tot}	$\mu_{\text{spin}}^{\text{eff}}$	μ_{orb}	μ_{mol}
$\{GdNi_8\}$	−0.02(2)	−0.02(2)	−0.04(4)	7.2(2)	0.8(2)	7.8(4)
$\{GdNi_8\} \cdot CH_3OH$	0.79(2)	0.09(2)	0.88(4)	7.4(2)	1.0(2)	15.4(4)
$\{TbNi_8\}$	0.10(2)	−0.01(2)	0.09(4)	2.7(2)	2.1(2)	6.4(4)
$\{TbNi_8\} \cdot CH_3OH$	0.23(2)	0.05(2)	0.29(4)	2.8(2)	2.5(2)	8.9(4)

and 2(d)]. The spectral feature of the Gd(III) XAS reflects the unoccupied $4f$ states that are hardly influenced by the chemical bonding because the $4f$ states are very localized. The satellite peaks observed in this case originate solely from the multiplet splitting caused by intraionic many-body interaction. The prominent negative XMCD peak at the M_5 edge (1185 eV) and the positive peak at the M_4 edge (1220 eV) indicate a large spin moment parallel to the external field.

For comparison, Fig. 3 shows the XAS and XMCD spectra of the $\{TbNi_8\}$ samples. In this case the XAS Ni L_3 edge at a photon energy of 853 eV also reveals two additional satellite peaks at 2 and 5 eV higher than the energy of the absorption maximum. However, the XAS spectra measured for the sample drop-cast from the dichloromethane solution [Fig. 3(a), case A] deviate only very little from the spectra measured for the same molecules drop-cast from a methanol solution [Fig. 3(c), case B]. For case A the satellite peak at 855 eV is smaller but the separation from the main peak is still larger (2.0 eV) compared to case B (1.9 eV).

The obvious difference for the Ni XMCD signal observed for the two $\{GdNi_8\}$ cases is also present for $\{TbNi_8\}$. In case A the XMCD signal is considerably smaller than the result for case B. However, for $\{TbNi_8\}$ we observe in both cases a prevailing spin moment parallel to the applied external field, but with a much smaller value for case A.

The XAS and XMCD signals measured at the Tb(III) $M_{5,4}$ edge are almost similar to each other for both cases A and B [Figs. 3(b) and 3(d)] for the same reason as the spectra for Gd(III). However, careful inspection of the M_5 maximum reveals a slightly more pronounced double peak for case A compared to case B. This small difference is discussed below. The prominent negative XMCD peak at the M_5 edge (1240 eV) and the almost-absent peak at the M_4 edge (1275 eV) indicates a large orbital moment in addition to the spin moment parallel to the external field.

We first discuss the magnetic moments of the Ni(II) ions resulting from the sum-rule analysis [70]. For Ni(II) the number of d holes is close to $n_h = 2$ according to the charge-transfer multiplet calculations. The effective spin moment deviates from the spin moment μ_{spin} according to $\mu_{\text{spin}}^{\text{eff}} = \mu_{\text{spin}} + 7T_z\,\mu_{\text{B}}$. In the case of transition metal ions the T_z term depends on the chemical bonding and cannot be calculated exactly. It has been shown that it may assume large values for adsorbed Cu phthalocyanine molecules [74]. On the other hand, the magnetic anisotropy related to the Ni(II) ion is expected to be small in view of the almost-quenched orbital magnetic moments. Therefore, the T_z contribution vanishes for a powder sample because of the averaging over all possible orientations, i.e., $\mu_{\text{spin}}^{\text{eff}} = \mu_{\text{spin}}$. Spin and orbital moments are summarized in Table I.

The Ni spin moment calculated for the $\{GdNi_8\}$ spectrum shown in Fig. 2(a) reveals almost-vanishing spin and orbital moments.

In the case of drop-casting from a methanol solution [Fig. 2(c)] the spin moment dramatically increases to almost $0.8\,\mu_{\text{B}}$ per Ni(II) ion. This is a very large value corresponding to almost half the maximum possible value for a Ni $3d^8$ configuration. A smaller value is expected considering the mutual antiferromagnetic exchange coupling between neighboring $3d$ transition metal ions, as, for example, observed in Ref. [65] for a similar molecular structure. The total molecular moment of $\{GdNi_8\}$ increases by a factor of 2 when the drop-casting solution is exchanged from dichloromethane to methanol.

For $\{TbNi_8\}$ we also observe an increase of the Ni moment comparing the samples drop-cast from a dichloromethane solution and a methanol solution. In this case, the increase of the total Ni moment is smaller than in the case of $\{GdNi_8\}$ but also amounts to a factor of three.

For the *RE* $3d \rightarrow 4f$ transitions a similar sum-rule analysis is performed. For Gd and Tb the numbers of unoccupied $4f$ states are $n_h = 7$ and 6, respectively. The effective spin moment comprises the true spin moment and a contribution from the expectation value of the dipole moment operator T_z, $\mu_{\text{spin}}^{\text{eff}} = \mu_{\text{spin}} + 6T_z\,\mu_{\text{B}}$. The contribution of T_z is negligible for Gd(III) but cannot be neglected in the case of Tb(III).

For the Gd(III) ion in $\{GdNi_8\}$ we get a spin moment close to the expected value of $7\,\mu_{\text{B}}$ according to Hund's rules $2S = 7$ and $L = 0$. Surprisingly the orbital moment does not vanish. As in the case of Gd(III) we have $\mu_{\text{spin}}^{\text{eff}} = \mu_{\text{spin}}$, and we can determine the total moment for the Gd(III) ion summing up the spin and orbital moments. A small increase by 5% of the total moment for the sample drop-cast from the methanol solution is observed in comparison to the total moment for the sample of case A.

The Tb(III) ion shows a spin moment that is considerably reduced compared to the expected ionic value, $2S = 6$ and $L = 3$. Following the model explained in Ref. [66], we assume that a strong magnetic anisotropy hinders the alignment of the

rare-earth magnetic moment with the external field. Exploiting the ratio r of the experimentally determined rare-earth orbital moment and the expected ionic value for Tb(III) of $3\,\mu_B$ we can determine the magnetic anisotropy assuming a powder average. Our experimental results are $r = 0.7$ and $r = 0.83$ for cases A and B, respectively. Following the procedure described in Ref. [66], we obtain the magnetic anisotropy constants $K_{RE}(\mathrm{Tb}) = 5.1$ meV and $K_{RE}(\mathrm{Tb}) = 2.9$ meV, respectively. From the ratio r one can also derive the correction for the T_z component of the effective spin moment. The spin moments of the Tb(III) ion are then $\mu_{\mathrm{spin}} = 3.8\,\mu_B$ and $\mu_{\mathrm{spin}} = 3.9\,\mu_B$ for cases A and B, respectively. The correction for the T_z contribution thus roughly restores the expected ratio of the spin moment and the orbital moment for Tb(III) of 2 : 1.

Considering all ionic moments contributing to the molecular moment we find that the total molecular moment increases by a factor of approximately 1.5 for $\{TbNi_8\}$ drop-cast from a methanol solution compared to the same molecule drop-cast from a dichloromethane solution.

IV. DISCUSSION

To explain the different results obtained for the same molecules dissolved in two different solvents, we first note that the experimental results for small single crystals glued by a conductive adhesive are similar to results for the metallacrowns dissolved in the noncoordinating solvent dichloromethane. In particular, both samples show very low values for the Ni magnetic moments. From x-ray diffraction of a single crystal we know that seven of the eight Ni(II) ions have four nearest-neighbor atoms, three oxygen and one nitrogen atom, arranged planar. One Ni(II) ion has an additional covalently bonded morpholin ligand. This coordination mode leads for at least seven Ni(II) ions to a ligand field that can be described approximately as a square-planar field. The square-planar ligand field is known to favor a low-spin state, i.e., $S = 0$. To confirm the low-spin state we performed charge-transfer multiplet calculations [72]. Figure 4(a) shows the simulated spectra with the ligand field parameters set to $10Dq = 1.8$ eV, $Ds = 0.6$ eV, and $Dt = 0.1$ eV, representing a square-planar geometry. The corresponding simulated XMCD signal almost vanishes (please note the factor 10 magnification), indicating vanishing magnetic spin and orbital moments confirming the low-spin state. The simulated XAS reproduces the experimentally observed spectra shown in Figs. 2(a) and 3(a), including the two satellite peaks.

The corresponding scheme of the splitting of the Ni(II) $3d$ orbitals is depicted in Fig. 1(b). The highest level representing the $d_{x^2-y^2}$ orbital is separated from the nearest lower level by 1.8 eV. This energy difference is larger than the correlation energy. Therefore, the energy difference favors the parallel orientation of the two spins in one orbital and the total spin is zero.

The attached methanol molecules exemplified in the sketch in Fig. 1(a) (site B) break the square-planar geometry, leading to a tetragonal extended or even octahedral ligand field. To simulate the corresponding spectra we set the ligand field parameters to $10Dq = 1.8$ eV, $Ds = 0.0$ eV, and $Dt = 0.0$ eV. These parameters lead to a strongly increased XMCD signal as shown in Fig. 4(b), indicating a high-spin state. The

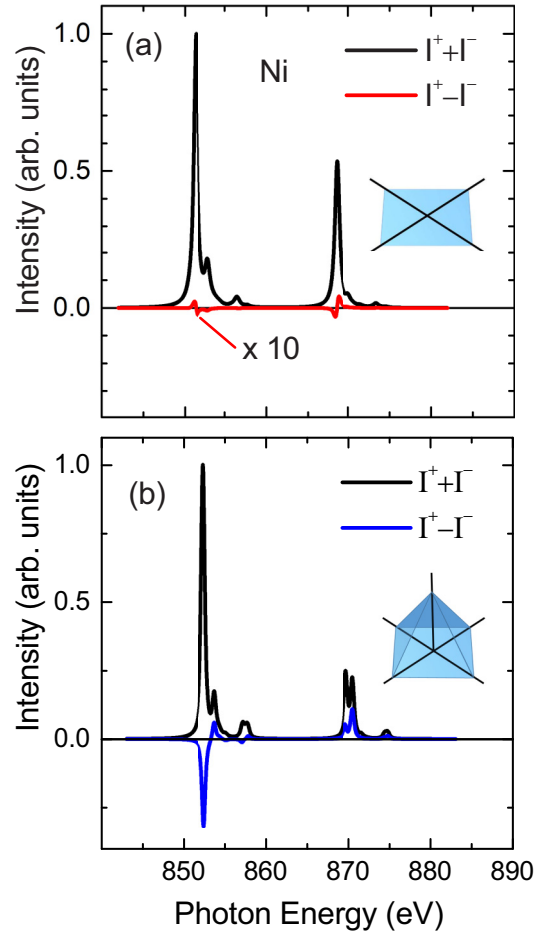

FIG. 4. (a) Ni(II) XAS and XMCD spectra simulated by charge-transfer multiplet calculations [72]. The ligand field parameters were set to $10Dq = 1.8$ eV, $Ds = 0.6$ eV, and $Dt = 0.1$ eV, representing a square-planar geometry. (b) Similar charge-transfer multiplet calculations with the ligand field parameters set to $10Dq = 1.8$ eV, $Ds = 0.0$ eV, and $Dt = 0.0$ eV, representing an octahedral geometry. The XAS for Ni(II) are normalized to the maximum value. The corresponding XMCD spectra are scaled by the same normalization factor. The Ni(II) XMCD spectra in panel (a) is magnified by a factor of 10.

spectral shape reproduces the experimentally observed XMCD spectra, in particular the prevailing negative peak at the L_3 edge followed by a small positive peak. The two positive peaks at the L_2 edge with increased intensity for the second peak show up in the simulation, too. The simulated XAS reveal the satellite peak at 1.8 eV higher than the absorption maximum as observed in the experiment. Furthermore, the L_2 absorption peak is split into two separated peaks. Although, this is not directly seen in the experiment, we have observed a clear broadening of this peak. The overall good agreement of simulated and experimentally observed spectra confirms the assumed change of the ligand field geometry due to the attached methanol molecules.

The corresponding scheme of the splitting of the Ni(II) $3d$ orbitals [Fig. 1(b)] reveals that the highest levels are formed by the $d_{x^2-y^2}$ and d_{z^2} orbitals. In this case, the energy difference between these two orbitals is smaller than the correlation energy. Consequently, the two orthogonal orbitals

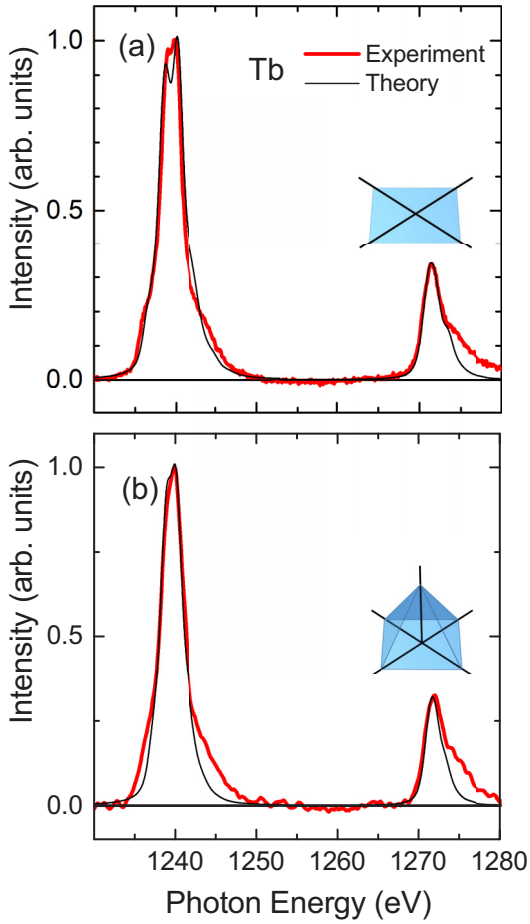

FIG. 5. (a) Tb(III) XAS simulated by multiplet calculations [72] (thin black line) compared to the corresponding experimental data for case A (low spin). The crystal field parameters have been set to zero. The Slater integral reduction has been set to 90% of the atomic value. (b) Similar multiplet calculations and experimental data for case B (high spin) with the Slater integral reduction has been set to 70% of the atomic value.

are occupied by two electrons with the same sign of the spin, representing a high-spin state, $S = 1$. The transition from the low-spin to the high-spin state occurs by reducing the parameter Ds below 0.3 eV.

While the x-ray absorption spectra of Gd(III) appear identical, the Tb(III) signal revealed small variations. The interaction of ligand fields and $4f$ orbitals of the rare-earth ions is very small and will not lead to visible changes of the spectral behavior [76]. On the other hand the methanol coordination may lead to changes in the hybridization strength, which in turn may be modeled by the Slater integral reduction in multiplet calculations. Variations on the order of 10% lead to similar spectral changes as observed in the experiment (see Fig. 5).

The experimental result for the $\{TbNi_8\}$ double-decker metallacrown reveals a small parallel Ni moment of $0.09\,\mu_B$ for case A (drop-cast from dichloromethane solution). The small remaining Ni moment may originate from the single Ni(II) ion with the additional morpholin ligand, although for $\{GdNi_8\}$ this Ni moment should also be present. Furthermore, the increase of the Ni moment upon drop-casting from the methanol solution ($0.3\,\mu_B$) is weaker than in the case of $\{GdNi_8\}$ ($0.9\,\mu_B$). The smaller Ni moment for $\{TbNi_8\}$ compared to $\{GdNi_8\}$ might be explained by a ferromagnetic exchange coupling to the central rare-earth ion as follows. The Ni(II)-Tb(III) exchange coupling is weaker and the mutual antiferromagnetic interaction of the Ni moments causes the reduction of the Ni(II) moment. The Ni(II)-Gd(III) exchange interaction is stronger mainly because of the larger Gd moment, thus leading to a parallel orientation of the Ni moments (magnetic director approach) [65].

V. SUMMARY

We have investigated element-specific magnetic spin and orbital magnetic moments of double-decker metallacrowns at low temperature (7 K) and in high-magnetic fields (7 T) using x-ray magnetic circular dichroism. The double-decker metallacrown molecules comprise one rare-earth metal Gd(III) or Tb(III) ion embedded between two squared scaffolds of four Ni(II) ions. The square-planar ligand field at the Ni(II) ion sites leads to an $S = 0$ ground state with vanishing Ni moments. Solving the double-decker metallacrowns in the coordinating solvent methanol leads to a considerable increase of the Ni magnetic moment, indicating a deviation from the square-planar ligand field. We attribute the moment increase to the attachment of methanol molecules at the Ni(II) ions. The additional methanol molecule leads to a change from the square-planar to a square-pyramidal ligand field, thus provoking a switch to an $S = 1$ ground state, corresponding to a spin crossover from a low-spin to a high-spin state. Charge-transfer multiplet calculations considering the different ligand field geometries confirm our experimental results.

Our results show that the low-spin state of Ni(II) ions originating from a square-planar ligand field is sensitive to distortions. Electrical fields from coordinating solution molecules may provoke a spin crossover to a high-spin state. On the other hand, this sensitivity can be exploited to control the spin state of the double-decker metallacrown without affecting the integrity of the molecule by chemical reactions.

ACKNOWLEDGMENTS

Excellent support by the staff of BESSY II is gratefully acknowledged. This work is supported by the German Research Foundation (DFG) through the Transregional Collaborative Research Center, SFB/TRR173 Spin+X, Project A09. Financial support for developing and building the PM2-VEKMAG beamline and the VEKMAG end station was provided by HZB and BMBF (Grants No. 05K10PC2, No. 05K10WR1, and No. 05K10KE1), respectively. Steffen Rudorff is acknowledged for technical support.

[1] K. S. Kumar and M. Ruben, Coord. Chem. Rev. **346**, 176 (2017).

[2] G. Molnar, L. Salmon, W. Nicolazzi, F. Terki, and A. Bousseksou, J. Mater. Chem. C **2**, 1360 (2014).

[3] S. Brooker, Chem. Soc. Rev. **44**, 2880 (2015).
[4] P. Gamez, J. S. Costa, M. Quesada, and G. Aromi, Dalton Trans., 7845 (2009).
[5] A. Gaspar, V. Ksenofontov, M. Seredyuk, and P. Gutlich, Coord. Chem. Rev. **249**, 2661 (2005).
[6] A. Gaspar, M. Seredyuk, and P. Gutlich, Coord. Chem. Rev. **253**, 2399 (2009).
[7] A. Gaspar and M. Seredyuk, Coord. Chem. Rev. **268**, 41 (2014).
[8] M. Halcrow, Chem. Soc. Rev. **40**, 4119 (2011).
[9] J.-F. Létard, P. Guionneau, and L. Goux-Capes, Towards spin crossover applications, *Spin Crossover in Transition Metal Compounds III*, Topics in Current Chemistry, Vol. 235 (Springer, Berlin, Heidelberg, 2004), pp. 221–249.
[10] M. Halcrow, Chem. Soc. Rev. **37**, 278 (2008).
[11] P. Gutlich, A. Hauser, and H. Spiering, Angew. Chem., Int. Ed. Engl. **33**, 2024 (1994).
[12] M. Nihei, T. Shiga, Y. Maeda, and H. Oshio, Coord. Chem. Rev. **251**, 2606 (2007).
[13] P. Gütlich and H. A. Goodwin, Editors, *Spin Crossover in Transition Metal Compounds I-III* (Springer, Berlin, 2004).
[14] M. Gruber, T. Miyamachi, V. Davesne, M. Bowen, S. Boukari, W. Wulfhekel, M. Alouani, and E. Beaurepaire, J. Chem. Phys. **146**, 092312 (2017).
[15] Y. Homma and T. Ishida, Chem. Mater. **30**, 1835 (2018).
[16] S. Venkataramani, U. Jana, M. Dommaschk, F. D. Sönnichsen, F. Tuczek, and R. Herges, Science **331**, 445 (2011).
[17] M. Halcrow, Crystals **6**, 58 (2016).
[18] H. Feltham, A. Barltrop, and S. Brooker, Coord. Chem. Rev. **344**, 25 (2017).
[19] K. Bairagi, O. Iasco, A. Bellec, A. Kartsev, D. Li, J. Lagoute, C. Chacon, Y. Girard, S. Rousset, F. Miserque, Y. Dappe, A. Smogunov, C. Barreteau, M.-L. Boillot, T. Mallah, and V. Repain, Nat. Commun. **7**, 12212 (2016).
[20] M. Shatruk, H. Phan, B. Chrisostomo, and A. Suleimenova, Coord. Chem. Rev. **289–290**, 62 (2015).
[21] R. Bertoni, M. Lorenc, A. Tissot, M.-L. Boillot, and E. Collet, Coord. Chem. Rev. **282–283**, 66 (2015).
[22] C. Lefter, V. Davesne, L. Salmon, G. Molnar, P. Demont, A. Rotaru, and A. Bousseksou, Magnetochemistry **2**, 18 (2016).
[23] Z.-P. Ni, J.-L. Liu, M. Hoque, W. Liu, J.-Y. Li, Y.-C. Chen, and M.-L. Tong, Coord. Chem. Rev. **335**, 28 (2017).
[24] C. F. Hermanns, M. Bernien, A. Krüger, W. Walter, Y.-M. Chang, E. Weschke, and W. Kuch, Phys. Rev. B **88**, 104420 (2013).
[25] P. Gambardella, S. Stepanow, A. Dmitriev, J. Honolka, F. M. F. de Groot, M. Lingenfelder, S. S. Gupta, D. D. Sarma, P. Bencok, S. Stanescu, S. Clair, S. Pons, N. Lin, A. P. Seitsonen, H. Brune, J. V. Barth, and K. Kern, Nat. Mater. **8**, 189 (2009).
[26] L. X. Chen, W. J. H. Jäger, G. Jennings, D. J. Gosztola, A. Munkholm, and J. P. Hessler, Science **292**, 262 (2001).
[27] H. Duval, V. Bulach, J. Fischer, and R. Weiss, Inorg. Chem. **38**, 5495 (1999).
[28] C. Wäckerlin, K. Tarafder, J. Girovsky, J. Nowakowski, T. Hählen, A. Shchyrba, D. Siewert, A. Kleibert, F. Nolting, P. M. Oppeneer, T. A. Jung, and N. Ballav, Angew. Chem., Int. Ed. **52**, 4568 (2013).
[29] A. Caneschi, D. Gatteschi, R. Sessoli, A. Barra, L. Brunel, and M. Guillot, J. Am. Chem. Soc. **113**, 5873 (1991).
[30] R. Sessoli, D. Gatteschi, A. Caneschi, and M. Novak, Nature (London) **365**, 141 (1993).
[31] D. Gatteschi, A. Caneschi, L. Pardi, and R. Sessoli, Science **265**, 1054 (1994).
[32] C. Cadiou, M. Murrie, C. Paulsen, V. Villar, W. Wernsdorfer, and R. Winpenny, Chem. Commun. **24**, 2666 (2001).
[33] J. Sokol, A. Hee, and J. Long, J. Am. Chem. Soc. **124**, 7656 (2002).
[34] C. J. Milios, R. Inglis, A. Vinslava, R. Bagai, W. Wernsdorfer, S. Parsons, S. P. Perlepes, G. Christou, and E. K. Brechin, J. Am. Chem. Soc. **129**, 12505 (2007).
[35] P.-H. Lin, T. J. Burchell, L. Ungur, L. F. Chibotaru, W. Wernsdorfer, and M. Murugesu, Angew. Chem., Int. Ed. **48**, 9489 (2009).
[36] I. J. Hewitt, J. Tang, N. T. Madhu, C. E. Anson, Y. Lan, J. Luzon, M. Etienne, R. Sessoli, and A. K. Powell, Angew. Chem., Int. Ed. **49**, 6352 (2010).
[37] Y.-N. Guo, G.-F. Xu, P. Gamez, L. Zhao, S.-Y. Lin, R. Deng, J. Tang, and H.-J. Zhang, J. Am. Chem. Soc. **132**, 8538 (2010).
[38] R. J. Blagg, C. A. Muryn, E. J. L. McInnes, F. Tuna, and R. E. P. Winpenny, Angew. Chem., Int. Ed. **50**, 6530 (2011).
[39] J. Long, F. Habib, P.-H. Lin, I. Korobkov, G. Enright, L. Ungur, W. Wernsdorfer, L. F. Chibotaru, and M. Murugesu, J. Am. Chem. Soc. **133**, 5319 (2011).
[40] C. Zaleski, E. Depperman, J. Kampf, M. Kirk, and V. Pecoraro, Angew. Chem., Int. Ed. **43**, 3912 (2004).
[41] S. Osa, T. Kido, N. Matsumoto, N. Re, A. Pochaba, and J. Mrozinski, J. Am. Chem. Soc. **126**, 420 (2004).
[42] J. Rinck, G. Novitchi, W. Van den Heuvel, L. Ungur, Y. Lan, W. Wernsdorfer, C. E. Anson, L. F. Chibotaru, and A. K. Powell, Angew. Chem., Int. Ed. **49**, 7583 (2010).
[43] M. Holynska, D. Premuzic, I.-R. Jeon, W. Wernsdorfer, R. Clerac, and S. Dehnen, Chem.-Euro. J. **17**, 9605 (2011).
[44] J. Dreiser, K. S. Pedersen, C. Piamonteze, S. Rusponi, Z. Salman, M. E. Ali, M. Schau-Magnussen, C. A. Thuesen, S. Piligkos, H. Weihe, H. Mutka, O. Waldmann, P. Oppeneer, J. Bendix, F. Nolting, and H. Brune, Chem. Sci. **3**, 1024 (2012).
[45] P. Happ, C. Plenk, and E. Rentschler, Coord. Chem. Rev. **289**, 238 (2015).
[46] Q.-W. Li, J.-L. Liu, J.-H. Jia, Y.-C. Chen, J. Liu, L.-F. Wang, and M.-L. Tong, Chem. Commun. **51**, 10291 (2015).
[47] C. M. Zaleski, S. Tricard, E. C. Depperman, W. Wernsdorfer, T. Mallah, M. L. Kirk, and V. L. Pecoraro, Inorg. Chem. **50**, 11348 (2015).
[48] J. D. Rinehart and J. R. Long, Chem. Science **2**, 2078 (2011).
[49] W. W. Lukens and M. D. Walter, Inorg. Chem. **49**, 4458 (2010).
[50] N. Ishikawa, M. Sugita, T. Okubo, N. Tanaka, T. Lino, and Y. Kaizu, Inorg. Chem. **42**, 2440 (2003).
[51] J. Luzon, K. Bernot, I. J. Hewitt, C. E. Anson, A. K. Powell, and R. Sessoli, Phys. Rev. Lett. **100**, 247205 (2008).
[52] M. Arrio, A. Scuiller, P. Sainctavit, C. Moulin, T. Mallah, and M. Verdaguer, J. Am. Chem. Soc. **121**, 6414 (1999).
[53] G. Champion, N. Lalioti, V. Tangoulis, M. Arrio, P. Sainctavit, F. Villain, A. Caneschi, D. Gatteschi, C. Giorgetti, F. Baudelet, M. Verdaguer, and C. Moulin, J. Am. Chem. Soc. **125**, 8371 (2003).
[54] R. Moroni, C. Cartier dit Moulin, G. Champion, M.-A. Arrio, P. Sainctavit, M. Verdaguer, and D. Gatteschi, Phys. Rev. B **68**, 064407 (2003).
[55] T. Hamamatsu, K. Yabe, M. Towatari, S. Osa, N. Matsumoto, N. Re, A. Pochaba, J. Mrozinski, J.-L. Gallani, A. Barla,

P. Imperia, C. Paulsen, and J.-P. Kappler, Inorg. Chem. **46**, 4458 (2007).

[56] G. Rogez, B. Donnio, E. Terazzi, J.-L. Gallani, J.-P. Kappler, J.-P. Bucher, and M. Drillon, Adv. Mater. (Weinheim, Ger.) **21**, 4323 (2009).

[57] R. Biagi, J. Fernandez-Rodriguez, M. Gonidec, A. Mirone, V. Corradini, F. Moro, V. De Renzi, U. del Pennino, J. C. Cezar, D. B. Amabilino, and J. Veciana, Phys. Rev. B **82**, 224406 (2010).

[58] M. Mannini, F. Pineider, C. Danieli, F. Totti, L. Sorace, P. Sainctavit, M. A. Arrio, E. Otero, L. Joly, J. C. Cezar, A. Cornia, and R. Sessoli, Nature (London) **468**, 417 (2010).

[59] V. Corradini, A. Ghirri, U. del Pennino, R. Biagi, V. A. Milway, G. Timco, F. Tuna, R. E. P. Winpenny, and M. Affronte, Dalton Trans. **39**, 4928 (2010).

[60] S. Stepanow, J. Honolka, P. Gambardella, L. Vitali, N. Abdurakhmanova, T.-C. Tseng, S. Rauschenbach, S. L. Tait, V. Sessi, S. Klyatskaya, M. Ruben, and K. Kern, J. Am. Chem. Soc. **132**, 11900 (2010).

[61] M. Prinz, K. Kuepper, C. Taubitz, M. Raekers, S. Khanra, B. Biswas, T. Weyhermueller, M. Uhlarz, J. Wosnitza, J. Schnack, A. V. Postnikov, C. Schroeder, S. J. George, M. Neumann, and P. Chaudhuri, Inorg. Chem. **49**, 2093 (2010).

[62] M. Gonidec, R. Biagi, V. Corradini, F. Moro, V. De Renzi, U. del Pennino, D. Summa, L. Muccioli, C. Zannoni, D. B. Amabilino, and J. Veciana, J. Am. Chem. Soc. **133**, 6603 (2011).

[63] M. Mannini, E. Tancini, L. Sorace, P. Sainctavit, M.-A. Arrio, Y. Qian, E. Otero, D. Chiappe, L. Margheriti, J. C. Cezar, R. Sessoli, and A. Cornia, Inorg. Chem. **50**, 2911 (2011).

[64] A. Lodi Rizzini, C. Krull, T. Balashov, J. J. Kavich, A. Mugarza, P. S. Miedema, P. K. Thakur, V. Sessi, S. Klyatskaya, M. Ruben, S. Stepanow, and P. Gambardella, Phys. Rev. Lett. **107**, 177205 (2011).

[65] P. Happ, A. Sapozhnik, J. Klanke, P. Czaja, A. Chernenkaya, K. Medjanik, S. Schuppler, P. Nagel, M. Merz, E. Rentschler, and H. J. Elmers, Phys. Rev. B **93**, 174404 (2016).

[66] A. Alhassanat, C. Gamer, A. Rauguth, A. A. Athanasopoulou, J. Sutter, C. Luo, H. Ryll, F. Radu, A. A. Sapozhnik, T. Mashoff, E. Rentschler, and H. J. Elmers, Phys. Rev. B **98**, 064428 (2018).

[67] A. Kredel, Auf Metallakronen basierende 3d-4f Sandwichkomplexe, Ph.D. thesis, Johannes Gutenberg University, Mainz, 2015.

[68] T. Noll and F. Radu, in Proceedings of MEDSI2016, p. 370, 2017.

[69] P. Carra, B. T. Thole, M. Altarelli, and X. Wang, Phys. Rev. Lett. **70**, 694 (1993).

[70] B. T. Thole, P. Carra, F. Sette, and G. van der Laan, Phys. Rev. Lett. **68**, 1943 (1992).

[71] G. Lorusso, V. Corradini, A. Candini, A. Ghirri, R. Biagi, U. del Pennino, S. Carretta, E. Garlatti, P. Santini, G. Amoretti, G. Timco, R. G. Pritchard, R. E. P. Winpenny, and M. Affronte, Phys. Rev. B **82**, 144420 (2010).

[72] E. Stavitski and F. M. F. de Groot, Micron **41**, 687 (2010).

[73] J. Crocombette, B. Thole, and F. Jollet, J. Phys.: Condens. Matter **8**, 4095 (1996).

[74] S. Stepanow, A. Mugarza, G. Ceballos, P. Moras, J. C. Cezar, C. Carbone, and P. Gambardella, Phys. Rev. B **82**, 014405 (2010).

[75] J. Stohr, J. Electron Spectrosc. Relat. Phenom. **75**, 253 (1995).

[76] V. Cuartero, S. Lafuerza, G. Subias, J. Garcia, E. Schierle, J. Blasco, and J. Herrero-Albillos, Phys. Rev. B **91**, 165111 (2015).